International Journal of Non-Linear Mechanics 47 (2012) 331–340

Contents lists available at ScienceDirect

International Journal of Non-Linear Mechanics

journal homepage: www.elsevier.com/locate/nlm

# A finite element approach to study cavitation instabilities in non-linear elastic solids under general loading conditions

Toshio Nakamura [a], Oscar Lopez-Pamies [b,*]

[a] Department of Mechanical Engineering, State University of New York, Stony Brook, NY 11794-2300, USA
[b] Department of Civil and Environmental Engineering, University of Illinois, Urbana-Champaign, IL 61801-2352, USA

ARTICLE INFO

Available online 28 July 2011

*Keywords:*
Defects
Voids and nucleation
Microstructure evolution
Bifurcation

ABSTRACT

This paper proposes an effective numerical method to study cavitation instabilities in non-linear elastic solids. The basic idea is to examine—by means of a 3D finite element model—the mechanical response under affine boundary conditions of a block of non-linear elastic material that contains a single infinitesimal defect at its center. The occurrence of cavitation is identified as the event when the initially small defect suddenly grows to a much larger size in response to sufficiently large applied loads. While the method is valid more generally, the emphasis here is on solids that are isotropic and defects that are vacuous and initially spherical in shape. As a first application, the proposed approach is utilized to compute the entire onset-of-cavitation surfaces (namely, the set of all critical Cauchy stress states at which cavitation ensues) for a variety of incompressible materials with different convexity properties and growth conditions. For strictly polyconvex materials, it is found that cavitation occurs only for stress states where the three principal Cauchy stresses are tensile and that the required hydrostatic stress component at cavitation increases with increasing shear components. For a class of materials that are not polyconvex, on the other hand and rather counterintuitively, the hydrostatic stress component at cavitation is found to decrease for a range of increasing shear components. The theoretical and practical implications of these results are discussed.



## 1. Introduction

It is known since the 1930s [1,2] that loading conditions with sufficiently large triaxialities can induce the sudden appearance of internal cavities within elastomeric solids.[1] The occurrence of such a phenomenon, termed cavitation, can be attributed to the sudden growth of pre-existing defects.[2] It was in this line of thought that Gent and Lindley [8] proposed to utilize the theory of finite elasticity to explain when and how cavitation actually occurs in elastomers. In essence, these authors examined the problem of radially symmetric deformation under external hydrostatic pressure of a non-linear elastic ball that contains an infinitesimal spherical cavity at its center. Assuming the ball to be made out of incompressible Neo-Hookean material and the cavity to be vacuous, they found that as the applied pressure approaches the critical value $P_{cr}=5\mu/2$ (with $\mu$ denoting the material shear modulus in the ground state), the size of the cavity suddenly becomes finite, and therefore cavitation ensues. Remarkably, this theoretical value has turned out to be in good agreement with a variety of experimental observations [7]. In a different approach, yet within the context of finite-elasticity theory, Ball [9] considered cavitation not as the growth of defects but rather as a class of non-smooth bifurcations, one in which cavities in the interior of defect-free materials are created once a critical external load is attained. For well-understood reasons [9–11], the above two approaches lead to identical critical applied pressures at which cavitation ensues in isotropic solids subjected to hydrostatic loading. This suggests that the phenomenon of cavitation in non-linear elasticity can be viewed rather equivalently as the sudden growth of pre-existing defects or as a non-smooth bifurcation in an initially defect-free material. Here, we closely follow the approach of Lopez-Pamies [12] and Lopez-Pamies et al. [13] and consider the phenomenon of cavitation as the growth of pre-existing defects.

The classical results of Gent and Lindley [8] and of Ball [9] are based on the restrictions that: (i) the applied loading is hydrostatic, (ii) the material behavior is incompressible and isotropic, and (iii) in the case of Gent and Lindley, the pre-existing defect is assumed to be a single vacuous spherical cavity, while in the

* Corresponding author.
*E-mail addresses:* toshio.nakamura@sunysb.edu (T.R. Nakamura), oscar.lopez-pamies@sunysb.edu (O. Lopez-Pamies).

[1] Cavitation instabilities have also been observed in other classes of materials including ductile metals [3], soft adhesives [4], gels [5], and biological tissues [6].

[2] In a typical elastomer, defects are expected to appear randomly distributed and to have a wide range of sizes with average diameters fluctuating around 0.1 μm. But beyond these geometrical features not much is known about their nature; they may possibly correspond to actual holes, particles of dust, and/or even weak regions of the polymer network [7].

0020-7462/$ - see front matter © 2011 Elsevier Ltd. All rights reserved.
doi:10.1016/j.ijnonlinmec.2011.07.007

analogous result of Ball, the formation of a single vacuous spherical cavity is the only bifurcation allowed in the analysis. Over the last three decades, numerous efforts have been devoted to extend these results to more general loading conditions, material behaviors, and types of defects/bifurcations, both by *analytical* and by *numerical* techniques. We refer to the reviews of Horgan and Polignone [14] and Fond [15], and to the more recent paper by Lopez-Pamies et al. [13] for an up-to-date account of contributions and remaining open problems on the *analytical* front. Among the first *numerical* efforts to study cavitation are those of Ball and Knowles [16],Hou and Abeyaratne [17], Chang et al. [18], and Negrón-Marrero and Bentacourt [19], who investigated a number of special cases in one and two dimensions. More recently, Xu and Henao [20] have proposed a more comprehensive approach based on a non-conforming finite element method that permits to study the case of compressible solids with multiple cavities under non-symmetric loading. In spite of these advances, a conspicuous lacuna that remains in the numerical analysis of cavitation is the study of three-dimensional (3D) problems.

The objective of the present paper is to introduce an effective numerical approach to study the onset of cavitation in non-linear elastic solids under arbitrary 3D loading conditions. The idea is to first consider the elastostatics problem of a block of non-linear elastic material that contains an infinitesimal non-linear elastic inhomogeneity or defect at its center and that is subjected to affine displacement boundary conditions. Numerical solutions are then generated by means of a finite element method. These include solutions for the change in volume of the underlying defect as a function of the applied loading, from which the onset of cavitation corresponding to the event when the (initially infinitesimal) defect suddenly grows to finite volume—can be readily determined. The distinctive features of this approach are that it: (i) allows to consider 3D general loading conditions with arbitrary triaxiality, (ii) is applicable to large classes of non-linear elastic solids, and (iii) directly accounts for the initial shape and mechanical properties of the underlying defect at which cavitation can initiate.

In regard to the above last feature, it is important to remark that (by considering only one defect) the proposed strategy neglects interactions among defects altogether. This is a simplifying assumption supported by recent calculations [20,21], which have suggested that the critical loads at which cavitation ensues in non-linear elastic solids are fairly insensitive to the number of underlying defects. Accounting for the presence of multiple defects becomes crucial, however, in the post-cavitation regime when the defects are no longer infinitesimal and therefore interact strongly and may even possibly coalesce.

For definiteness, the emphasis of this paper will be on solids that are isotropic and defects that are vacuous and initially spherical in shape; the more laborious cases of anisotropic materials and non-vacuous defects of more complex shapes will be considered elsewhere. As a first application of both theoretical and practical interest, we concentrate in particular on computing the entire onset-of-cavitation surfaces for a variety of incompressible materials with different convexity properties and growth conditions. These results aim at providing—for the first time—quantitative insight into how load triaxiality and material behavior affect the onset of cavitation in non-linear elastic solids.

The structure of the paper is as follows. In Section 2, we cast the problem of cavitation as the problem of the growth of a defect within a non-linear elastic solid in response to sufficiently large applied external loads. Section 2.1 discusses the specialization to isotropic solids and vacuous spherical defects. In Section 3, we present a finite element approach to construct numerical solutions for the problem formulated in Section 2. This approach is then utilized in Section 4 to compute onset-of-cavitation surfaces for various incompressible materials with different convexity properties and growth conditions. Finally, Section 5 provides some concluding remarks.

## 2. Problem setting: cavitation as the sudden growth of defects

Consider a single inhomogeneity or defect embedded in the geometric center of an otherwise homogeneous block of material. In its undeformed stress-free configuration, this two-phase solid occupies a volume $\Omega_0=\Omega_0^{(1)}\bigcup\Omega_0^{(2)}$ with boundary $\partial\Omega_0$, where $\Omega_0^{(1)}$ and $\Omega_0^{(2)}$ denote, respectively, the subdomains occupied by the "matrix" material and the defect. Material points in the solid are identified by their initial position vector $\mathbf{X}\in\Omega_0$, while the current position vector of the same point in the deformed configuration $\Omega$ is given by $\mathbf{x}=\boldsymbol{\chi}(\mathbf{X})$. Motivated by physical arguments, the mapping $\boldsymbol{\chi}$ is required to be twice continuously differentiable (except possibly on the defect boundary, where it is only required to be continuous) and one-to-one on $\Omega_0$. The deformation gradient $\mathbf{F}$ at $\mathbf{X}$ is defined by

$$\mathbf{F}=\mathrm{Grad}\,\boldsymbol{\chi},\quad J=\det\mathbf{F}>0\quad\text{in}\quad\Omega_0. \tag{1}$$

Both the matrix ($r=1$) and the defect ($r=2$) are taken to be non-linear elastic solids characterized by non-convex stored-energy functions $W^{(r)}$ of $\mathbf{F}$, which are required to be non-negative, objective, and to linearize properly. The present analysis is thus general enough to allow for non-vacuous defects characterized by some non-zero stored-energy function $W^{(2)}$. At each material point $\mathbf{X}$ in the undeformed configuration, the first Piola–Kirchhoff stress $\mathbf{S}$ is related to the deformation gradient $\mathbf{F}$ by

$$\mathbf{S}=\frac{\partial W}{\partial\mathbf{F}}(\mathbf{X},\mathbf{F}),\quad W(\mathbf{X},\mathbf{F})=(1-\theta_0(\mathbf{X}))\,W^{(1)}(\mathbf{F})+\theta_0(\mathbf{X})\,W^{(2)}(\mathbf{F}), \tag{2}$$

where $\theta_0$ is the characteristic function that takes the value 1 if the position vector $\mathbf{X}\in\Omega_0^{(2)}$, and 0 otherwise, and serves therefore to describe the geometry of the defect in the undeformed configuration $\Omega_0$. Of particular importance here is the geometric quantity

$$f_0=\frac{|\Omega_0^{(2)}|}{|\Omega_0|}=\frac{1}{|\Omega_0|}\int_{\Omega_0}\theta_0(\mathbf{X})\,\mathrm{d}\mathbf{X}, \tag{3}$$

which measures the initial volume fraction (i.e., the initial overall size) of the defect.

We suppose now that the block is subjected to the affine displacement boundary condition

$$\mathbf{x}=\overline{\mathbf{F}}\mathbf{X}\quad\text{on}\ \partial\Omega_0, \tag{4}$$

where the second-order tensor $\overline{\mathbf{F}}$ is a prescribed constant quantity. In the absence of body forces, it follows that the total elastic energy (per unit undeformed volume) stored in the material is given by

$$E=\min_{\mathbf{F}\in\mathcal{K}(\overline{\mathbf{F}})}\frac{1}{|\Omega_0|}\int_{\Omega_0}W(\mathbf{X},\mathbf{F})\,\mathrm{d}\mathbf{X}, \tag{5}$$

where $\mathcal{K}$ denotes a suitable set of kinematically admissible deformation gradient fields, and the associated equilibrium equations are in turn given by

$$\mathrm{Div}\left[\frac{\partial W}{\partial\mathbf{F}}(\mathbf{X},\mathbf{F})\right]=\mathbf{0}\quad\text{in}\ \Omega_0. \tag{6}$$

We also record here that the volume fraction of the defect in the deformed configuration reads simply as

$$f=\frac{|\Omega^{(2)}|}{|\Omega|}=\frac{f_0}{J}\frac{1}{|\Omega_0^{(2)}|}\int_{\Omega_0^{(2)}}\det\mathbf{F}(\mathbf{X})\,\mathrm{d}\mathbf{X}, \tag{7}$$

where $\Omega^{(2)}$ stands for the domain occupied by the defect in the deformed configuration and $\mathbf{F}(\mathbf{X})$ is the minimizing field in (5).

In the limit as $f_0 \to 0+$, the material under consideration in the above elastostatics problem reduces to a non-linear elastic solid with stored-energy function $W^{(1)}$ containing a *zero-volume defect* with stored-energy function $W^{(2)}$ and shape described by $\theta_0$. When the material is finitely deformed according to (4), the size of this defect (as measured by its volume fraction $f$ in the deformed configuration) can suddenly grow to finite values, signaling the onset of cavitation. The analysis of cavitation in non-linear elasticity amounts thus (see [13, Section 2]) to examining the asymptotic behaviors of the total elastic energy (5) and current volume fraction of defect (7) in the limit as $f_0 \to 0+$. In the next section, we present a finite element approach that will allow us to construct numerical solutions for $E$ and $f$ in such a limit.

### 2.1. The case of isotropic materials and vacuous spherical defects

Before proceeding with the construction of solutions, it is appropriate to emphasize that the above problem formulation is valid for any non-linear elastic matrix material (as characterized by $W^{(1)}$) and any non-linear elastic defect of arbitrary initial shape (as characterized by $W^{(2)}$ and $\theta_0$). In this work, the primary focus will be on matrix materials that are *isotropic* and defects that are *vacuous* and initially *spherical* in shape. These specifications imply that the stored-energy function $W^{(1)}$ can be conveniently expressed as a function of the principal invariants $I_1 = \mathrm{tr}\mathbf{C}$, $I_2 = \frac{1}{2}[(\mathrm{tr}\mathbf{C})^2 - \mathrm{tr}\mathbf{C}^2]$, $J = \sqrt{\det \mathbf{C}}$ of the right Cauchy–Green deformation tensor $\mathbf{C} = \mathbf{F}^T\mathbf{F}$, or, alternatively, as a symmetric function of the singular values $\lambda_1$, $\lambda_2$, $\lambda_3$ of $\mathbf{F}$:

$$W^{(1)}(\mathbf{F}) = \varphi(I_1, I_2, J) = \phi(\lambda_1, \lambda_2, \lambda_3), \tag{8}$$

where $\phi$ is symmetric. They further imply that

$$W^{(2)}(\mathbf{F}) = 0 \quad \text{and} \quad \theta_0(\mathbf{X}) = \begin{cases} 1 & \text{if } (\mathbf{X}-\mathbf{X}_0)\cdot(\mathbf{X}-\mathbf{X}_0) \le a_0^{1/2}, \\ 0 & \text{otherwise,} \end{cases} \tag{9}$$

where $a_0$ and $\mathbf{X}_0$ stand for, respectively, the radius and the spatial location of the center of the defect in the undeformed configuration. In view of the isotropy of the constitutive and geometric relations (8)–(9), it follows that the corresponding total elastic energy $E$ and current volume fraction of defect $f$ (as defined by expressions (5) and (7)) are isotropic functions of the applied boundary data $\overline{\mathbf{F}}$. When carrying out calculations for this case, it will then suffice to restrict attention to pure stretch loadings of the diagonal form:

$$\overline{F}_{ij} = \mathrm{diag}(\overline{\lambda}_1, \overline{\lambda}_2, \overline{\lambda}_3). \tag{10}$$

Consistent with this notation, the affine principal Cauchy stresses resulting on the outer boundary of the block $\partial\Omega_0$ (i.e., the far-field stresses) will be similarly denoted by $\overline{t}_1$, $\overline{t}_2$, $\overline{t}_3$. To better reveal the role of load triaxiality, we will also make use of the following alternative stress quantities:

$$\sigma_m \doteq \frac{1}{3}(\overline{t}_1 + \overline{t}_2 + \overline{t}_3), \quad \tau_1 \doteq \overline{t}_2 - \overline{t}_1, \quad \tau_2 \doteq \overline{t}_3 - \overline{t}_1. \tag{11}$$

Here, the mean stress $\sigma_m$ provides a measure of the hydrostatic loading on the boundary of the block, while $\tau_1$ and $\tau_2$ provide a measure of the shear loading. Larger values of $|\tau_1|$ and $|\tau_2|$ correspond to lower load triaxiality and represent a greater departure from a state of pure hydrostatic stress.

## 3. Finite element approach

In the sequel, we propose a finite element (FE) procedure to construct numerical solutions for (5) and (7) in the limit as $f_0 \to 0+$, from which we can then determine the onset of cavitation in non-linear elastic solids under general loading conditions. Attention is restricted to the case of isotropic materials (8) and vacuous spherical defects (9). Section 3.1 describes the construction of the FE model utilized to carry out the relevant calculations. This includes the selection of the geometry of the block, the size of the defect, the mesh discretization, and the type of finite elements. The numerical method of solution of (5) and (7) is explained in Section 3.2. Section 3.3 describes the process of computing the onset-of-cavitation surfaces as defined by the set of all critical loads at which cavitation ensues. We conclude (Section 3.4) with a brief discussion of the deformed shape of the defect at cavitation.

### 3.1. The FE model

Without loss of generality, we begin by choosing the block of material $\Omega_0$ containing the defect to be a cube of side $L_0$. While the geometry of the block is ultimately immaterial, a cubic geometry proves convenient for a more direct implementation of the boundary conditions (4) with (10). Also for convenience, we write the components of all tensorial quantities with respect to a Cartesian frame of reference whose origin is placed at the center of the cube, so that $\mathbf{X}_0 = \mathbf{0}$, and whose axes are aligned with the principal axes of the cube. The spatial region occupied by the block in the undeformed configuration can thus be written as

$$\Omega_0 = \left\{ \mathbf{X} \middle| -\frac{L_0}{2} \le X_i \le \frac{L_0}{2} \quad (i = 1,2,3) \right\}. \tag{12}$$

Given that the size of the defect in the FE model must be necessarily *finite*, we next need to identify how small its initial volume fraction $f_0 = 4\pi a_0^3/3L_0^3$ ought to be in order to accurately approximate an actual infinitesimal defect with $f_0 \to 0+$. To this end, we carried out a parametric study with decreasing values of initial volume fractions in the range $10^{-6} \le f_0 \le 10^{-12}$. For the type of materials of interest in this work, the results indicate that defects with $f_0 \le 10^{-8}$ are sufficiently small to be representative of an infinitesimal defect. Accordingly, in this work we set the initial volume fraction at

$$f_0 = \frac{\pi}{6} \times 10^{-9}, \tag{13}$$

corresponding to a defect of radius $a_0 = 1$ in a cube of side $L_0 = 2000$.

Having identified the geometries of the block and of the defect, we now turn to their discretization. In this regard, we note that the symmetry of the problem allows to perform the calculations in just one octant of the cube, $\Omega_0^l = \{\mathbf{X} | 0 \le X_i \le L_0/2 \quad (i = 1,2,3)\}$ say. A mesh generator code is used to construct the 3D geometry for such an octant, as depicted in Fig. 1. Here the mesh is designed so that the small elements are placed near the defect at uniform angular intervals of 2.25°, while the radial element sizes are gradually increased toward the outer boundary. In all, the mesh consists of 64,800 brick elements (with 1,200 elements in each radial plane and 54 layers in the radial direction). This discretization was selected after various mesh refinements were tried to assess accuracy. We also tested meshes with different discreteness along both angular and radial directions to confirm sufficient mesh convergence.

With the objective of being able to study cavitation in both compressible and incompressible materials, we make use of hybrid 8-node linear elements; higher order elements (e.g., quadratic 20-node elements) are not suitable for the present problem because of the extremely large deformations involved. Such hybrid elements treat the hydrostatic component of the stress as an interpolated basic solution variable and as a result can handle exactly (in a numerical sense) the strongly non-linear constraint of incompressibility. Since

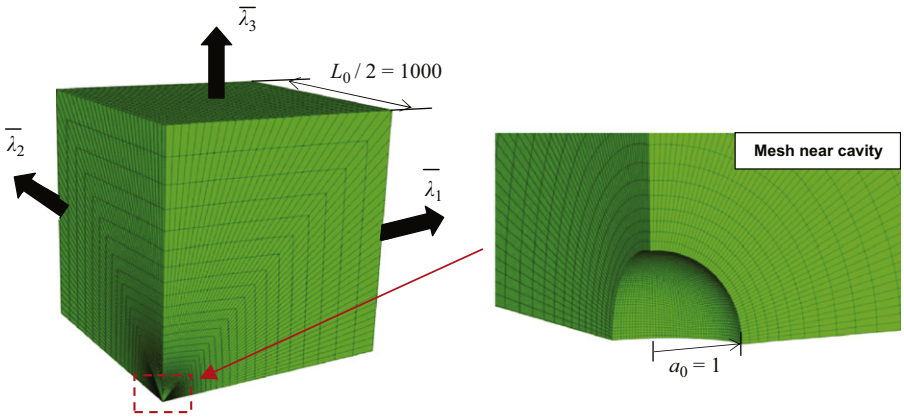


**Fig. 1.** Finite element model—in the undeformed configuration—of a small vacuous spherical defect of radius $a_0=1$ located at the center of a cubic block of side $L_0=2000$. The outer boundary of the cube is subjected to affine stretches $\overline{\lambda}_1, \overline{\lambda}_2, \overline{\lambda}_3$ aligned with the three principal axes of the cube. The affine principal Cauchy stresses resulting on the outer boundary of the cube are similarly denoted by $\overline{t}_1, \overline{t}_2, \overline{t}_3$.

the computations are carried using the FE package ABAQUS, we make use in particular of the C3D8H hybrid elements available in this code (see ABAQUS Version 6.9 Documentation [22]).

### 3.2. The numerical method of solution

A convenient way to implement the affine boundary conditions (4) with (10) is to follow radial straining paths in principal logarithmic strain space ($\overline{\varepsilon}_i = \ln \overline{\lambda}_i$). Specifically, we set

$$\overline{\lambda}_1 = \lambda^{\cos\Theta \sin\Psi}, \quad \overline{\lambda}_2 = \lambda^{\sin\Theta \sin\Psi}, \quad \overline{\lambda}_3 = \lambda^{\cos\Psi}, \tag{14}$$

where $\lambda \geq 1$ is the monotonically increasing load parameter of the deformation process, which takes the value of 1 in the undeformed configuration, and $\Theta \in [0,2\pi]$ and $\Psi \in [0,\pi]$ are the load path angles. Any desired macroscopic deformation state $(\overline{\lambda}_1,\overline{\lambda}_2,\overline{\lambda}_3)$ can be accessed by marching along (starting at $\lambda = 1$) radial paths (14) with appropriate fixed values of the angles $\Theta$ and $\Psi$.

For a given radial path (14), the FE calculations are carried out by gradually increasing the load parameter $\lambda$ from 1 to the desired final value; for the classes of materials to be studied here, the smallest required step size in the gradual increase of $\lambda$ is $\Delta\lambda = 10^{-8}$, but much larger steps in the order of $\Delta\lambda = 10^{-4}$ are often sufficient to reach convergence. At each step in such a loading path, the incremental equilibrium equations are solved directly (i.e., no direct energy minimization is carried out) in ABAQUS. We utilize the default dual convergence criterion in this code, namely, we check for the convergence of the ratio of the largest solution correction to the largest corresponding incremental solution value, as well as for the convergence of the ratio of the largest residual to the corresponding average flux norm (see ABAQUS Version 6.9 Documentation).

At this point, it is important to remark that because of the non-convexity of $W^{(1)}$ in $\mathbf{F}$, the solution to the equilibrium equations (6) need not be unique. However, given that $W^{(1)}$ is required to linearize properly, the minimization (5) is expected to yield a well-posed linearly elastic problem with a unique solution within a sufficiently small neighborhood of $\lambda = 1$. As the deformation progresses beyond the linearly elastic neighborhood into the finite deformation regime, the material may reach a point at which this unique solution bifurcates into different energy solutions. Our numerical solution corresponds to one of these equilibrium solutions, but need not necessarily correspond to the global energy-minimizing solution.

### 3.3. Computation of the onset-of-cavitation surfaces

Along a given loading path (14), the current volume fraction of the defect (7) in the above-described FE model may suddenly grow to finite values signaling the onset of cavitation. Because the initial size of the defect is small but not vanishingly so ($f_0 = \pi/6 \times 10^{-9}$), however, its sudden growth does *not* occur abruptly at a single load, but instead it occurs smoothly over a small range of loads. This behavior is illustrated in Fig. 2 for the case of a Neo-Hookean material under hydrostatic loading ($\overline{\lambda}_1 = \overline{\lambda}_2 = \overline{\lambda}_3 = \lambda \geq 1$), where the volume fraction $f$ (part (a)) and the normalized volume fraction $f/f_0$ (part (b)) of defect are plotted versus the hydrostatic Cauchy stress $\sigma_m$ on the outer boundary of the cube. The figure clearly shows that the volume fraction of the defect $f$ remains unchanged in the order of $f_0 = \pi/6 \times 10^{-9}$ until the far-field hydrostatic stress approaches the value of $2.5\mu$, just before which the defect begins to grow very rapidly but *smoothly*. For definiteness, in this work we shall consider that whenever the volume fraction of defect $f$ in the FE model, as defined by expression (7), increases five orders of magnitudes reaching the critical value:

$$f_{cr} = 10^5 \times f_0 = \frac{\pi}{6} \times 10^{-4}, \tag{15}$$

cavitation ensues.

The following remarks regarding the numerical cavitation criterion (15) are in order. The set of all critical triplets $(\overline{\lambda}_1^{cr},\overline{\lambda}_2^{cr},\overline{\lambda}_3^{cr})$ of principal stretches $(\overline{\lambda}_1,\overline{\lambda}_2,\overline{\lambda}_3)$ satisfying condition (15) defines an *onset-of-cavitation surface* $\mathcal{C}(\overline{\lambda}_1,\overline{\lambda}_2,\overline{\lambda}_3) = 0$ in deformation space. Similarly, the set of critical triplets $(\overline{t}_1^{cr},\overline{t}_2^{cr},\overline{t}_3^{cr})$ of the corresponding principal Cauchy stresses $(\overline{t}_1,\overline{t}_2,\overline{t}_3)$ on the outer boundary of the cube defines an *onset-of-cavitation surface* $\mathcal{S}(\overline{t}_1,\overline{t}_2,\overline{t}_3) = 0$ in stress space. Again, such surfaces can be computed by marching along (starting at $\lambda = 1$) radial paths (14) in $(\overline{\lambda}_1,\overline{\lambda}_2,\overline{\lambda}_3)$-space until the condition (15) is satisfied. It is also important to remark that using criteria different than a five-orders-of-magnitude increase—such as a four-orders-of-magnitude increase $f_{cr} = 10^4 \times f_0$ or a six-orders-of-magnitude increase $f_{cr} = 10^6 \times f_0$—leads to somewhat different values for the critical loads at which cavitation occurs, yet the qualitative character of the results remains unaltered. As a reference, we also note that the criterion (15) leads to a critical pressure of $\sigma_m = 2.46\mu$ for the onset of cavitation in a Neo-Hookean material under hydrostatic loading, in comparison to the classical result of $\sigma_m = 2.5\mu$ based on the solution for $f_0 \to 0+$.

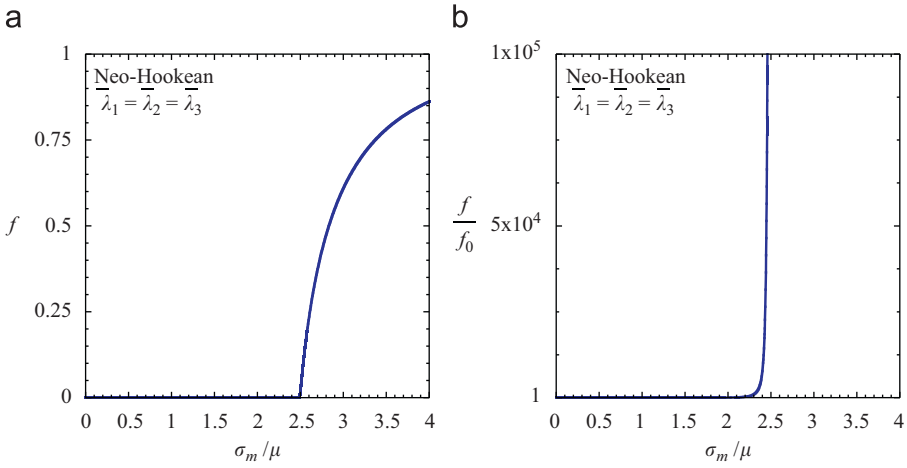


**Fig. 2.** Increase in the volume fraction $f$ (part (a)) and normalized volume fraction $f/f_0$ (part (b)) of defect in the FE model, as a function of the far-field hydrostatic Cauchy stress $\sigma_m$, for the case of a Neo-Hookean material under hydrostatic loading with $\bar{\lambda}_1=\bar{\lambda}_2=\bar{\lambda}_3=\lambda\geq 1$.

*3.3.1. The case of incompressible materials*

For the physically relevant case of incompressible materials with stored-energy function[3]:

$$W^{(1)}(\mathbf{F})=\begin{cases}\varphi(I_1,I_2,J)=\phi(\lambda_1,\lambda_2,\lambda_3) & \text{if } J=\lambda_1\lambda_2\lambda_3=1,\\ +\infty & \text{otherwise,}\end{cases} \tag{16}$$

the current volume fraction of defect (7) reduces to the *purely kinematical* expression:

$$f=1-\frac{1-f_0}{\bar{\lambda}_1\bar{\lambda}_2\bar{\lambda}_3}. \tag{17}$$

In view of this *explicit* result, it is trivial to deduce from the criterion (15) that cavitation occurs in the FE model at critical values $\bar{\lambda}_1^{cr},\bar{\lambda}_2^{cr},\bar{\lambda}_3^{cr}$ of the applied stretches $\bar{\lambda}_1,\bar{\lambda}_2,\bar{\lambda}_3$ such that

$$\bar{\lambda}_1^{cr}\bar{\lambda}_2^{cr}\bar{\lambda}_3^{cr}=\bar{J}_{cr}\doteq\frac{1-f_0}{1-f_{cr}}=\frac{1-\frac{\pi}{6}\times 10^{-9}}{1-\frac{\pi}{6}\times 10^{-4}}\approx 1.0000523621. \tag{18}$$

That is, the onset-of-cavitation surface in deformation space is simply given by $\mathcal{C}(\bar{\lambda}_1,\bar{\lambda}_2,\bar{\lambda}_3)=\bar{\lambda}_1\bar{\lambda}_2\bar{\lambda}_3-\bar{J}_{cr}=0$, irrespectively of the specific choice of stored-energy function (16).

The more insightful critical values $\bar{t}_1^{cr},\bar{t}_2^{cr},\bar{t}_3^{cr}$—which, unlike the critical stretches, will depend on the specific choice of stored-energy function (16)—of the corresponding stresses $\bar{t}_1,\bar{t}_2,\bar{t}_3$ at which cavitation ensues can be found by following radial loading paths (14) in $(\bar{\lambda}_1,\bar{\lambda}_2,\bar{\lambda}_3)$–space until the product $\bar{\lambda}_1\bar{\lambda}_2\bar{\lambda}_3$ reaches the value (18). An alternative, more efficient strategy is to first subject the cube to hydrostatic loading until condition (18) is reached, and then vary the ratios of the stretches $\bar{\lambda}_1/\bar{\lambda}_2$ and $\bar{\lambda}_2/\bar{\lambda}_3$ while keeping their product fixed at the cavitated state $\bar{\lambda}_1\bar{\lambda}_2\bar{\lambda}_3=\bar{J}_{cr}$ in such a way that the critical stresses $\bar{t}_1^{cr},\bar{t}_2^{cr},\bar{t}_3^{cr}$ are computed continuously along the loading path. A convenient parameterization of this two-step loading process is as follows:

$$\text{Step I}: \quad \bar{\lambda}_1=\bar{\lambda}_2=\bar{\lambda}_3=\lambda \quad \text{for } 1\leq\lambda\leq\bar{J}_{cr}^{1/3} \tag{19}$$

and

$$\text{Step II}: \quad \bar{\lambda}_1=\lambda,\quad \bar{\lambda}_2=\lambda^m,\quad \bar{\lambda}_3=\bar{J}_{cr}\lambda^{-(1+m)} \quad \text{for } \lambda>\bar{J}_{cr}^{1/3}, \tag{20}$$

where, similar to (14), $\lambda$ is a monotonically increasing load parameter that takes the value of 1 in the undeformed configuration and $m\in\mathbb{R}$, but because of symmetry it actually suffices to restrict attention to $m\in[-0.5,1]$.

To illustrate the above two-step strategy, Fig. 3 depicts sample FE solutions for the case of a one-term Ogden material with stored-energy function (29) and $\beta=1.5$. Part (a) shows results for the hydrostatic stress $\sigma_m$ on the outer boundary of the cube as a function of the load parameter $\lambda$ during Step I of the loading process. Results for Step II are shown for the case of $m=0.25$ in part (b), where the principal stresses $\bar{t}_1$, $\bar{t}_2$, $\bar{t}_3$ on the boundary of the cube are plotted as functions of $\lambda$. Part (c) shows more results for Step II for the cases of $m=-0.5,\ -0.25,\ 0,\ 0.25,\ 0.5,\ 0.75,\ 1$ in terms of the hydrostatic stress $\sigma_m$ as a function of the load parameter $\lambda$. Finally, part (d) shows the combined results of Step I and Step II for the hydrostatic stress $\sigma_m$ as a function of the shear stresses $\tau_1=\bar{t}_2-\bar{t}_1$ and $\tau_2=\bar{t}_3-\bar{t}_1$ (recall the definition (11)) for the cases of $m=-0.5,\ -0.25,\ 0,\ 0.25,\ 0.5,\ 0.75,\ 1$. Note that the stresses associated with Step II here correspond precisely to the critical stresses at which cavitation ensues. The entire onset-of-cavitation surface $\mathcal{S}(\bar{t}_1,\bar{t}_2,\bar{t}_3)=0$ can then be constructed by simply interpolating between these results and exploiting the inherent symmetries $\mathcal{S}(\bar{t}_1,\bar{t}_2,\bar{t}_3)=\mathcal{S}(\bar{t}_1,\bar{t}_3,\bar{t}_2)=\mathcal{S}(\bar{t}_2,\bar{t}_1,\bar{t}_3)=\mathcal{S}(\bar{t}_3,\bar{t}_1,\bar{t}_2)=\mathcal{S}(\bar{t}_2,\bar{t}_3,\bar{t}_1)=\mathcal{S}(\bar{t}_3,\bar{t}_2,\bar{t}_1)$ due to the overall isotropy of the problem.

*3.4. The deformed shape of the defect at cavitation*

In addition to providing results for the current *volume* fraction of the defect in the deformed configuration—from which the entire onset-of-cavitation surfaces can be constructed, as described in the preceding subsection—the proposed FE approach also provides results for the deformed *shape* of the defect. This further geometrical information can be utilized to better understand how cavitation takes place.

For demonstration purposes, Fig. 4 shows sample solutions for the deformed shape of the defect in the FE model for the case of the incompressible Ogden material (29) with $\beta=1.5$. The results correspond to cavitated states—so that, as dictated by Eq. (18), the stretches applied on the boundary of the cube satisfy the onset-of-cavitation condition $\bar{\lambda}_1\bar{\lambda}_2\bar{\lambda}_3=\bar{J}_{cr}$—computed by following loading paths of the form (20). Parts (a) and (c) show results for axisymmetric "compression" (i.e., $\bar{\lambda}_2=\bar{\lambda}_3<1$) and "tension" (i.e., $\bar{\lambda}_1=\bar{\lambda}_2>1$), while part (b) displays results for an intermediate non-axisymmetric ($\bar{\lambda}_1>\bar{\lambda}_2>\bar{\lambda}_3$)loading path. These markedly non-spherical results provide an unequivocal indication that the occurrence of cavitation in non-linear elastic solids depends

[3] Subsequently, the unbounded branch of incompressible stored-energy functions for non-isochoric deformations will be omitted for notational simplicity.

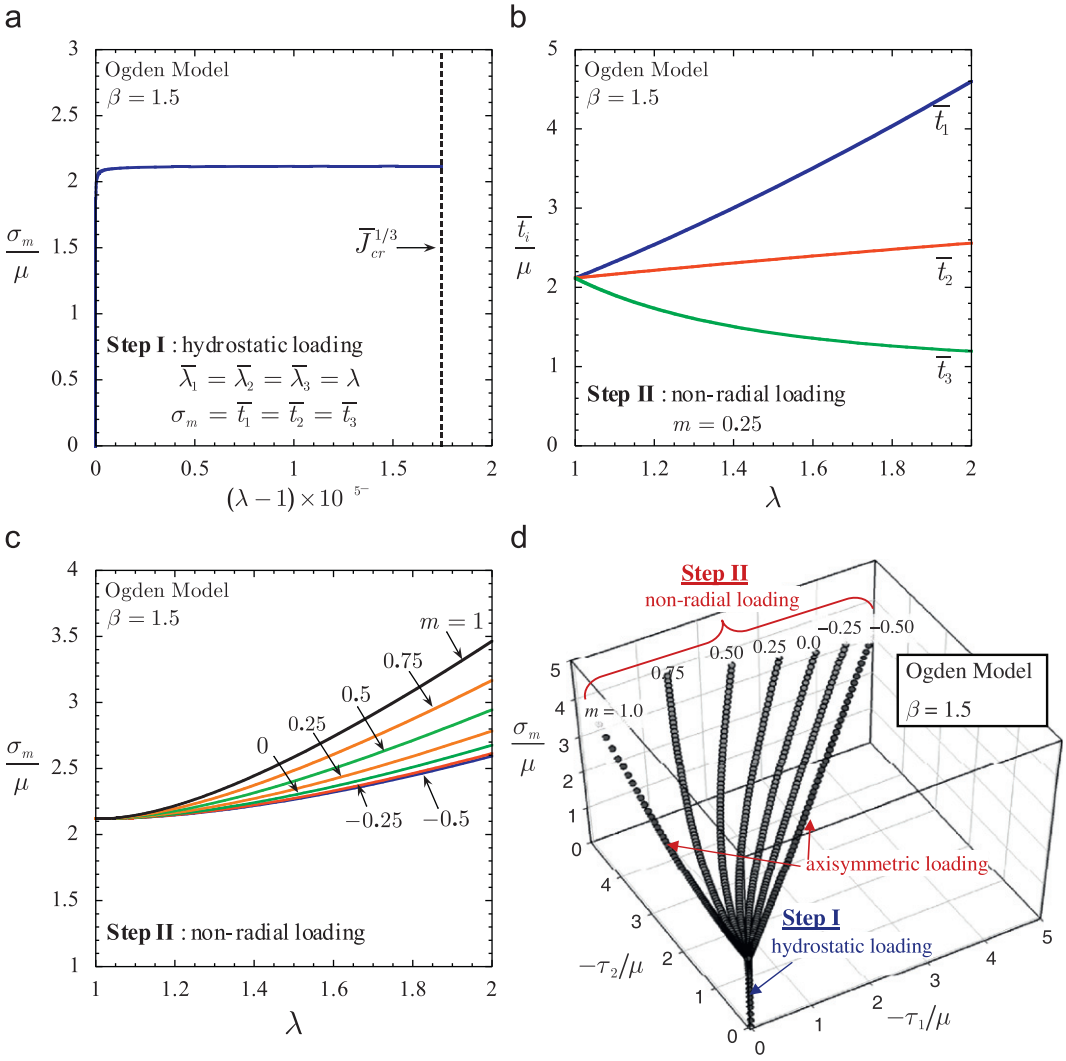


**Fig. 3.** FE solutions generated by marching along the two-step loading process (19)–(20) for the case of a one-term Ogden material (29) with $\beta = 1.5$. Part (a) shows results for the hydrostatic stress $\sigma_m$ as a function of the load parameter $\lambda$ during Step I. Parts (b) and (c) show results during Step II for the principal Cauchy stresses $\overline{t}_1, \overline{t}_2, \overline{t}_3$ and hydrostatic stress $\sigma_m$ versus $\lambda$ for various values of the parameter $m \in [-0.5, 1]$. Part (d) displays the combined results of Step I and Step II in the $(\sigma_m, \tau_1, \tau_2)$-stress space. The stresses associated with Step II correspond to the critical stresses at which cavitation ensues.

sensitively on the triaxiality of the applied loading, and not just on its hydrostatic component.

## 4. Application to incompressible materials with different convexity properties and growth conditions

In this section, we apply the above procedure to two classes of incompressible material models with the main objective of gaining quantitative insight into how load triaxiality and material behavior affect the onset of cavitation in non-linear elastic solids. For conciseness, attention is restricted to the onset-of-cavitation surfaces, results for the deformed shape of the defect at cavitation will be examined elsewhere. Specifically, we consider the popular Ogden [23] material model with stored-energy function:

$$\phi_{OG}(\lambda_1,\lambda_2,\lambda_3) = \sum_{r=1}^{N} \frac{2}{\beta_r^2} \nu_r (\lambda_1^{\beta_r} + \lambda_2^{\beta_r} + \lambda_3^{\beta_r} - 3) \tag{21}$$

and the more recent model proposed by Lopez-Pamies [24]

$$\varphi_{LP}(I_1) = \sum_{r=1}^{M} \frac{3^{1-\alpha_r}}{2\alpha_r} \mu_r (I_1^{\alpha_r} - 3^{\alpha_r}), \tag{22}$$

where $\nu_r$, $\beta_r$ and $\mu_r$, $\alpha_r$ are real-valued material parameters. These choices are particularly attractive for our purposes here because their convexity properties and growth conditions can be widely and expediently modulated by suitably modifying the values of their material parameters. The stored-energy functions (21) and (22) have the further merit that they have been shown to describe reasonably well the response of a variety of elastomers over large ranges of deformations.

For later reference, we remark that in the limit of small deformations as $\mathbf{F} \to \mathbf{I}$ the above energies linearize properly reducing to

$$\phi_{OG}(\lambda_1,\lambda_2,\lambda_3) = \sum_{r=1}^{N} \frac{\nu_r}{2} (\lambda_1^2 + \lambda_2^2 + \lambda_3^2 - 3) + O(\|\mathbf{F}-\mathbf{I}\|^3) \tag{23}$$

and

$$\varphi_{LP}(I_1) = \sum_{r=1}^{M} \frac{\mu_r}{2} (I_1 - 3) + O(\|\mathbf{F}-\mathbf{I}\|^3), \tag{24}$$

from which we deduce the connections $\sum_r^N \nu_r = \mu$ and $\sum_r^M \mu_r = \mu$ between the material parameters $\nu_r$ and $\mu_r$ and the shear modulus $\mu$ in the ground state. For large deformations, on the other hand, the parameters $\beta_r$ and $\alpha_r$ control the growth

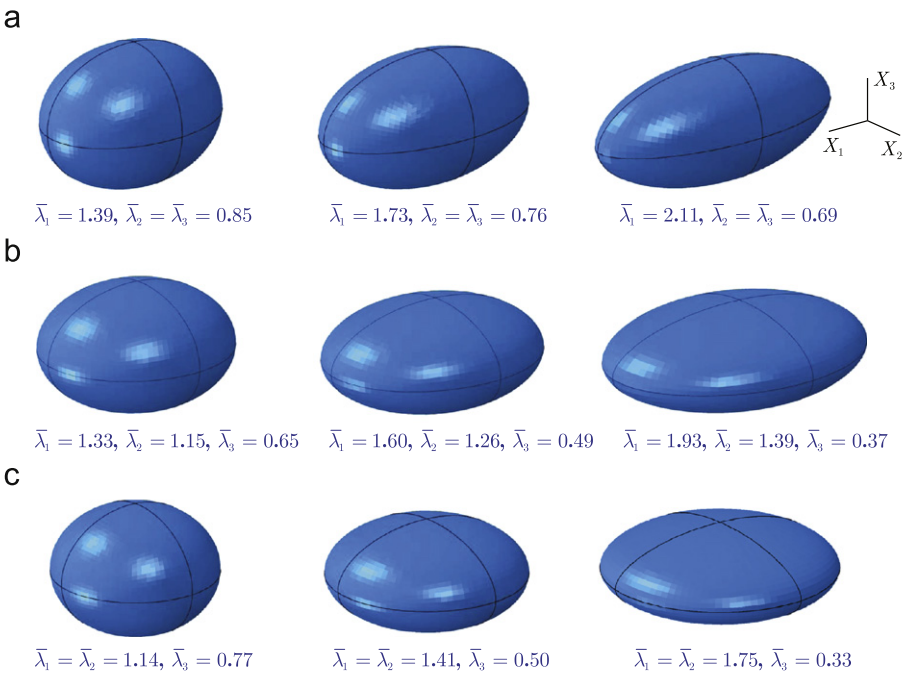


**Fig. 4.** Snapshots of the deformed shape of the defect at cavitation for various load triaxialities; namely, for various triplets $(\overline{\lambda}_1, \overline{\lambda}_2, \overline{\lambda}_3)$ of applied principal stretches satisfying the onset-of-cavitation condition $\overline{\lambda}_1\overline{\lambda}_2\overline{\lambda}_3 = \overline{J}_{cr}^{1/3}$. Consistent with Fig. 3, the sample results shown here correspond to the case of the incompressible Ogden material (29) with $\beta = 1.5$.

conditions of (21) and (22); in particular, the larger the values of $\beta_r$ and $\alpha_r$ the stronger the growth conditions (provided, of course that the corresponding $\nu_r$ and $\mu_r$ are positive).

Also for later reference, we record that *sufficient conditions*[4] for the Ogden stored-energy function (21) to be strictly polyconvex read as (see [26, Theorem 5.2])

$$\nu_r > 0 \quad \text{and} \quad \beta_r > 1 \quad (r = 1,2,\ldots,N). \tag{25}$$

*Necessary and sufficient conditions* for (22) to be strictly polyconvex, on the other hand, are given by the inequalities (see [24, Section 3.1]):

$$\varphi'_{LP}(I_1) > 0 \quad \text{and} \quad \varphi'_{LP}(I_1) + 2I_1\varphi''_{LP}(I_1) > 0, \tag{26}$$

where

$$\varphi'_{LP}(I_1) = \sum_{r=1}^{M} \frac{3^{1-\alpha_r}}{2}\mu_r I_1^{\alpha_r - 1} \quad \text{and} \quad \varphi''_{LP}(I_1) = \sum_{r=1}^{M} \frac{3^{1-\alpha_r}(\alpha_r - 1)}{2}\mu_r I_1^{\alpha_r - 2}. \tag{27}$$

Unfortunately, necessary and sufficient conditions on the parameters $\mu_r$ and $\alpha_r$ that ensure that (22) is strictly polyconvex do not exist. But it is straightforward to deduce from (26) that the conditions

$$\mu_r > 0 \quad \text{and} \quad \alpha_r > \tfrac{1}{2} \quad (r = 1,2,\ldots,M) \tag{28}$$

are *sufficient*. Since strict polyconvexity implies strong ellipticity, the explicit restrictions (25) and (28) are also sufficient to ensure the strong ellipticity of the stored-energy functions (21) and (22), respectively.

Because of the prominent role that polyconvexity plays in the majority of available theoretical studies of cavitation (see, e.g., [9,27,28]), in the next subsection we will present onset-of-cavitation surfaces for specific choices of materials (21) and (22) that are strictly polyconvex. In Section 4.2, motivated by experimental results, we will also present onset-of-cavitation surfaces for materials (22) that are *not* polyconvex, but that are stable in the sense that they are strongly elliptic. In this regard, it is fitting to remark that although desirable on a mathematical basis, the constitutive restriction of polyconvexity has not yet been given a strict physical interpretation and therefore its enforcement is arguable. On the other hand, the strong ellipticity condition must be enforced in general, since—consistent with experimental evidence on elastomeric solids—it entails physically that localized deformations (e.g., shear bands) cannot occur.

### 4.1. Onset-of-cavitation surfaces for strictly polyconvex materials

In this subsection we consider the one-term (i.e., $N=1$ and $M=1$) forms of the models (21) and (22):

$$\phi_{OG}(\lambda_1,\lambda_2,\lambda_3) = \frac{2}{\beta^2}\mu(\lambda_1^\beta + \lambda_2^\beta + \lambda_3^\beta - 3) \tag{29}$$

and

$$\varphi_{LP}(I_1) = \frac{3^{1-\alpha}}{2\alpha}\mu(I_1^\alpha - 3^\alpha), \tag{30}$$

with material parameters $\beta = 2,1.5,1.1$ for $\phi_{OG}$ and $\alpha = 1,0.8,0.6$ for $\varphi_{LP}$. Note that expressions (29) and (30) have the same shear modulus $\mu$ in the ground state (i.e., they linearize to the same material). Note further that for the cases of $\beta = 2$ and $\alpha = 1$, (29) and (30) reduce identically to the classical Neo-Hookean stored-energy function, which is strictly polyconvex. According to conditions (25) and (28), the cases $\beta = 1.5,1.1$ and $\alpha = 0.8,0.6$ correspond to materials that are also strictly polyconvex, but have weaker growth conditions than the Neo-Hookean material.

We begin by presenting onset-of-cavitation results for the Ogden material (29). Fig. 5(a) shows the entire onset-of-cavitation surface for the case of $\beta = 1.5$. The surface is plotted in terms of the hydrostatic stress $\sigma_m$ as a function of the shear stresses $\tau_1$ and $\tau_2$ at which cavitation ensues (recall the definition (11)). A key

[4] While necessary and sufficient conditions for polyconvexity of isotropic stored-energy functions written in terms of the principal stretches $\lambda_1,\lambda_2,\lambda_3$ have been provided by Mielke [25], they turn out to be fairly untractable when specialized to the Ogden stored-energy function (21).

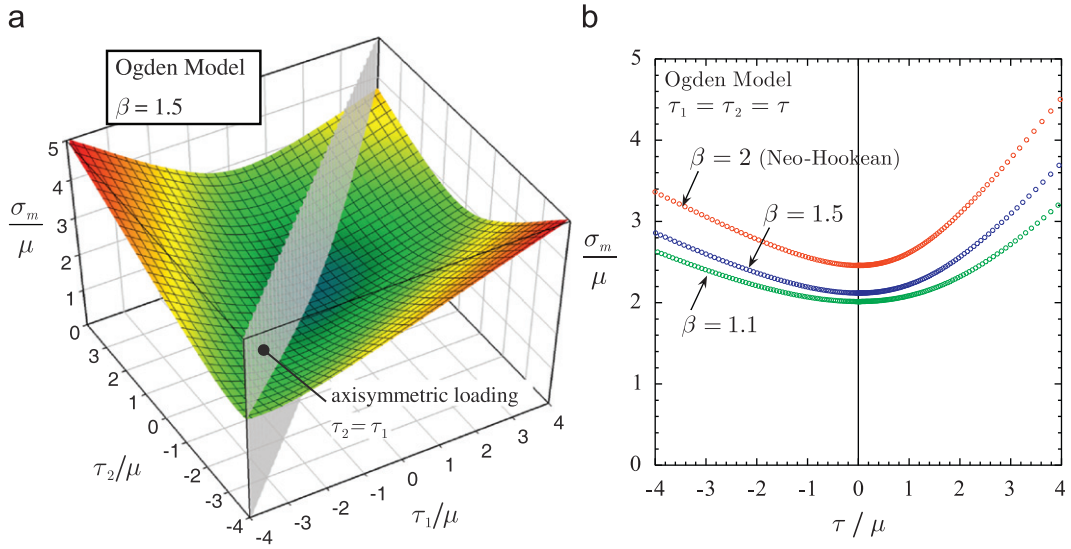


**Fig. 5.** (a) 3D plot of the onset-of-cavitation surface for the Ogden material (29) with $\beta = 1.5$ in the space of $(\sigma_m, \tau_1, \tau_2)$-stress. (b) Onset-of-cavitation curves for the Ogden material (29) under axisymmetric loading with $\tau_1 = \tau_2 = \tau$ in the space of $(\sigma_m, \tau)$-stress for three different values of the material parameter $\beta$.

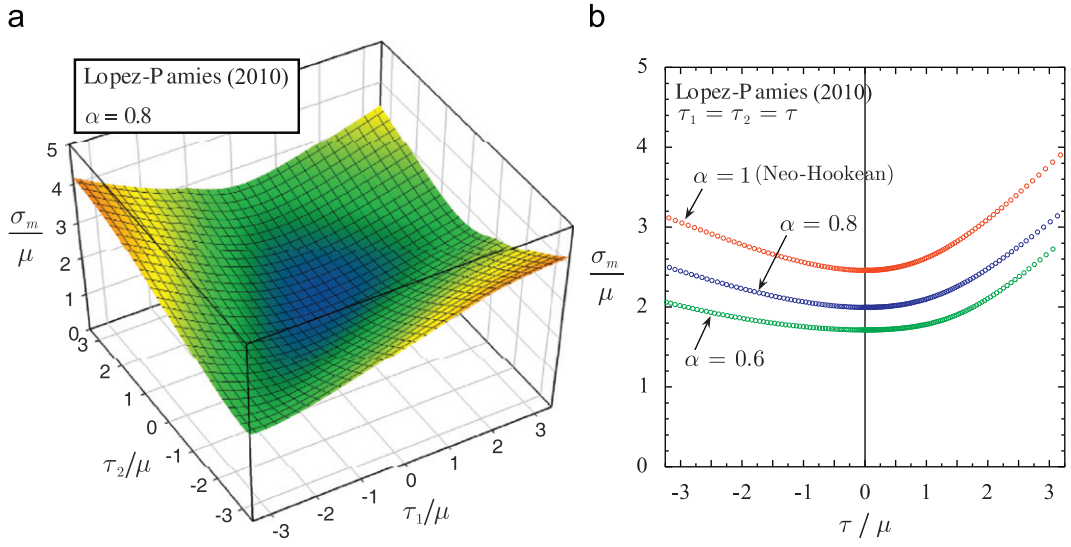


**Fig. 6.** (a) 3D plot of the onset-of-cavitation surface for the material model (30) with $\alpha = 0.8$ in the space of $(\sigma_m, \tau_1, \tau_2)$-stress. (b) Onset-of-cavitation curves for the material model (30) under axisymmetric loading with $\tau_1 = \tau_2 = \tau$ in the space of $(\sigma_m, \tau)$-stress for three different values of the material parameter $\alpha$.

observation from Fig. 5(a) is that cavitation occurs only at states of stress for which the hydrostatic part $\sigma_m$ is *tensile*, in accordance with experiments. Moreover, the critical value of $\sigma_m$ is lowest for purely hydrostatic loading when $\tau_1 = \tau_2 = 0$, and increases significantly and monotonically as the shear stresses $\tau_1$ and $\tau_2$ deviate from zero in any radial path, that is, as the load triaxiality decreases.

To aid in the visualization of the above-identified features, Fig. 5(b) shows the results along the axisymmetric loading plane with $\tau_2 = \tau_1 = \tau$. The plot also includes the results for $\beta = 2$ and 1.1. Again, for all three results, the critical value of $\sigma_m$ is seen to be lowest for purely hydrostatic loading when $\tau = 0$ and to increase significantly and monotonically as the shear stress $\tau$ deviates from zero. Interestingly, the critical $\sigma_m$ increases faster for loadings with $\tau > 0$, which correspond to the case when the two principal Cauchy stresses that are equal ($\bar{t}_2$ and $\bar{t}_3$ in this case) are greater than the other principal Cauchy stress ($\bar{t}_1$ in this case). It is also interesting to remark that weaker growth conditions (as characterized by lower values of $\beta$) uniformly shift the onset-of-cavitation curve to lower levels of hydrostatic stress but do not change its form.

Fig. 6 shows analogous results for the material model (30): part (a) shows the entire onset-of-cavitation surface for the case of $\alpha = 0.8$, while part (b) shows the onset-of-cavitation curves for $\alpha = 1, 0.8$, and 0.6 along axisymmetric loading conditions. The results are very much identical to those shown in Fig. 5 for the Ogden material. Note in particular from part (b) that weaker growth conditions (as characterized by lower values of $\alpha$ here) do not change the form of the onset-of-cavitation curve, but they uniformly shift it to lower levels of hydrostatic stress.

### 4.2. Onset-of-cavitation surfaces for strongly elliptic materials that are not polyconvex

We consider next the two-term ($M=2$) form of the stored-energy function (22):

$$\varphi_{LP}(I_1) = \frac{3^{1-\alpha_1}}{2\alpha_1}\mu_1(I_1^{\alpha_1} - 3^{\alpha_1}) + \frac{3^{1-\alpha_2}}{2\alpha_2}\mu_2(I_1^{\alpha_2} - 3^{\alpha_2}), \tag{31}$$

with material parameters $\mu_1 = 0.54\mu$, $\mu_2 = 0.46\mu$, $\alpha_1 = 0.6$, and $\alpha_2 = -68.73, -10, -1$, and 0.51. The case with $\alpha_2 = -68.73$

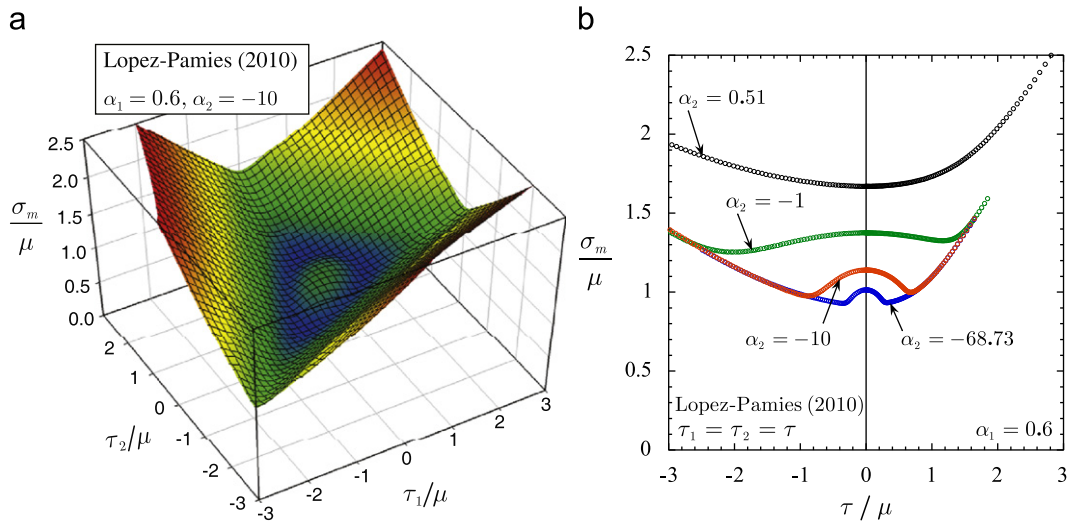


**Fig. 7.** (a) 3D plot of the onset-of-cavitation surface in the space of $(\sigma_m,\tau_1,\tau_2)$-stress for the material model (31) with $\mu_1 = 0.54\mu$, $\mu_2 = 0.46\mu$, $\alpha_1 = 0.6$, and $\alpha_2 = -10$. (b) Corresponding onset-of-cavitation curves under axisymmetric loading with $\tau_1 = \tau_2 = \tau$ in the space of $(\sigma_m,\tau)$-stress for four different values of the material parameter $\alpha_2$.

corresponds to a stored-energy function that was fitted to the response of a commercial elastomer synthesized by the tire company Michelin, as discussed in Section 2.3 of [24]. It is easy to verify from conditions (26) that such an energy is not polyconvex. It is, however, strongly elliptic (see [24, Section 3.1]) and thus macroscopically stable. The cases with $\alpha_2 = -10$ and $-1$ correspond also to stored-energy functions that are strongly elliptic but *not* polyconvex, whereas the stored-energy function with $\alpha_2 = 0.51$ is strictly polyconvex (and thus strongly elliptic); these last three cases are not associated with experimental data, but have been selected to facilitate the discussion.

We do not consider the corresponding two-term ($N=2$) form of the Ogden model (21) here because the untractability of the available *necessary and sufficient* conditions for its polyconvexity makes is difficult to choose values for $\nu_r$ and $\beta_r$ that result in stored-energy functions that are strongly elliptic but not polyconvex, which is precisely the case of interest in this subsection. As hinted to above, this is in contrast to the stored-energy function (22) for which *necessary and sufficient* conditions for its polyconvexity (see Eq. (26)) and strong ellipticity (see [24, Eq. (22)] and [29, Section 4]) are remarkably simple.

Fig. 7(a) shows the onset-of-cavitation surface for the material model (31) with $\alpha_2 = -10$ in terms of the hydrostatic stress $\sigma_m$ as a function of the shear stresses $\tau_1$ and $\tau_2$. Similar to the previous results, cavitation is seen to occur only at states of stress for which the hydrostatic part $\sigma_m$ is tensile. As opposed to the previous results, however, the critical value of $\sigma_m$ is *not* lowest for purely hydrostatic loading when $\tau_1 = \tau_2 = 0$. Instead, and rather counterintuitively, $\sigma_m$ *decreases* monotonically as the shear stresses $\tau_1$ and $\tau_2$ deviate from zero in any radial path before reaching a minimum, after which $\sigma_m$ reverses trends and monotonically increases with further increase in $\tau_1$ and $\tau_2$. In other words, within a neighborhood of the purely hydrostatic state of stress, the material becomes less stable—in the sense that cavitation takes place at lower hydrostatic stresses—with decreasing load triaxiality. For states of stress with sufficiently low triaxialities, the trend is reversed and the material improves its stability with further decreasing load triaxiality.

Fig. 7(b) shows the results along axisymmetric loading conditions ($\tau_2 = \tau_1 = \tau$). For comparison purposes, the plot also includes the results for $\alpha_2 = -68.73, -1$, and 0.51. From this "two-dimensional" perspective, it is clearly seen that $\sigma_m$ does indeed first decrease, then reaches a minimum, and eventually increases as $\tau$ deviates from zero. This same counterintuitive trend is exhibited by the two other materials, $\alpha_2 = -68.73$ and $\alpha_2 = -1$ that are not polyconvex. By contrast, the material that is strictly polyconvex, $\alpha_2 = 0.51$, exhibits a behavior that is fully consistent with the polyconvex materials examined in the preceding subsection. These results then suggest, rather interestingly, that it is the condition (or lack) of polyconvexity what dictates whether or not isotropic non-linear elastic solids improve their stability with decreasing load triaxiality.

We conclude this section by making contact with some experimental observations. In the contexts of filled elastomers [30–33] and structures bonded by soft adhesives [4], the regions surrounding the inherent soft/stiff interfaces are known to develop high stress triaxialities and therefore are prone to cavitation. Yet the stress states in these regions are *not* purely hydrostatic but do involve sizable shear stresses. According to the results presented above, predictions based upon radially symmetric cavitation ignoring the effect of shear stresses in these materials systems—as often done in the literature—may then result in substantial errors, and may even lead to incorrect conclusions. In the context of rubber-toughened polymers [34,35], the underlying rubber particles also develop states of high (but not purely) hydrostatic stress. Ignoring the effect of shear stresses on the onset of cavitation in this case may also lead to incorrect conclusions.

## 5. Concluding remarks

In this paper, a defect-growth approach has been proposed to study numerically the onset of cavitation in non-linear elastic solids subjected to 3D loading conditions with arbitrary triaxiality. While the strategy applies more generally, the emphasis has been on isotropic materials and on vacuous spherical defects. The more laborious cases of anisotropic materials and defects of more complex constitutive behaviors and shapes will be considered in future work.

As a first application, the approach was utilized to construct onset-of-cavitation surfaces for two fairly general classes of incompressible isotropic materials. The results indicated that both, the applied load triaxiality and the material convexity properties and growth conditions, play a significant role on when and how cavitation ensues. In particular, they showed that

polyconvex materials consistently improve their stability, in the sense that they cavitate at larger values of hydrostatic stress, when subjected to lower triaxiality loadings. The results also showed that materials that are not polyconvex, on the contrary, can become less stable and cavitate at smaller values of hydrostatic stress when subjected to loadings with lower triaxiality.

The growth of a cavitating defect within a real elastomer is expected to eventually lead to the fracture of the underlying polymer chains surrounding the defect [7]. It would be interesting to extend the strategy presented here to account for this transition from cavitation to fracture (see, e.g., the work of Williams and Schapery [36]).

## Acknowledgments

This work was supported by the National Science Foundation through Grants DMS–1009503 and CMMI–1055528.

## References

[1] W.F. Busse, Physics of rubber as related to the automobile, J. Appl. Phys. 9 (1938) 438–451.
[2] F.L. Yerzley, Adhesion of neoprene to metal, Ind. Eng. Chem. 31 (1939) 950–956.
[3] M.F. Ashby, F.J. Blunt, M. Bannister, Flow characteristics of highly constrained metal wires, Acta Metall. 37 (1989) 1847–1857.
[4] C. Creton, J. Hooker, Bulk and interfacial contributions to the debonding mechanisms of soft adhesives: extension to large strains, Langmuir 17 (2001) 4948–4954.
[5] S. Kundu, A.J. Crosby, Cavitation and fracture behavior of polyacrylamide hydrogels, Soft Matter 5 (2009) 3963–3968.
[6] A. Goriely, D.E. Moulton, R. Vandiver, Elastic cavitation, tube hollowing, and differential growth in plants and biological tissues, Euro. Phys. Lett. 91 (2010) 18001.
[7] A.N. Gent, Cavitation in rubber: A cautionary tale, Rubber Chem. Technol. 63 (1991) G49–G53.
[8] A.N. Gent, P.B. Lindley, Internal rupture of bonded rubber cylinders in tension, Proc. R. Soc. London A 249 (1959) 195–205.
[9] J.M. Ball, Discontinuous equilibrium solutions and cavitation in nonlinear elasticity, Philos. Trans. R. Soc. A 306 (1982) 557–611.
[10] J. Sivaloganathan, Uniqueness of regular and singular equilibria for spherically symmetric problems of nonlinear elasticity, Arch. Ration. Mech. Anal. 96 (1986) 97–136.
[11] J. Sivaloganathan, S.J. Spector, V. Tilakraj, The convergence of regularized minimizers for cavitation problems in nonlinear elasticity, SIAM J. Appl. Math. 66 (2006) 736–757.
[12] O. Lopez-Pamies, Onset of cavitation in compressible, isotropic, hyperelastic solids, J. Elasticity 94 (2009) 115–145.
[13] O. Lopez-Pamies, M.I. Idiart, T. Nakamura, Cavitation in elastomeric solids: I – A defect-growth theory, J. Mech. Phys. Solids 59 (2011) 1464–1487.
[14] C.O. Horgan, D.A. Polignone, Cavitation in nonlinearly elastic solids: a review, Appl. Mech. Rev. 48 (1995) 471–485.
[15] C. Fond, Cavitation criterion for rubber materials: a review of void-growth models, J. Polym. Sci.: Part B 39 (2001) 2081–2096.
[16] J.M. Ball, G. Knowles, A numerical method for detecting singular minimizers, Numer. Math. 51 (1987) 181–197.
[17] H.-S. Hou, R. Abeyaratne, Cavitation in elastic and elastic-plastic solids, J. Mech. Phys. Solids 40 (1992) 571–592.
[18] Y.-W. Chang, A.N. Gent, J. Padovan, Expansion of a cavity in a rubber block under unequal stresses, Int. J. Fract. 60 (1993) 283–291.
[19] P.V. Negrón-Marrero, O. Bentacourt, The numerical computation of singular minimizers in two-dimensional elasticity, J. Comput. Phys. 113 (1994) 291–303.
[20] X. Xu, D. Henao, An efficient numerical method for cavitation in nonlinear elasticity. Math. Models Methods Appl. Sci., in press, doi:10.1142/S0218202511005556.
[21] O. Lopez-Pamies, T. Nakamura, M.I. Idiart, Cavitation in elastomeric solids: II – Onset-of-cavitation surfaces for Neo-Hookean materials, J. Mech. Phys. Solids 59 (2011) 1488–1505.
[22] ABAQUS Version 6.9 Documentation, Dassault Systèmes Simulia Corp., Providence, RI, USA, 2009.
[23] R.W. Ogden, Large deformation isotropic elasticity – on the correlation of theory and experiment for incompressible rubberlike solids, Proc. R. Soc. London A 326 (1972) 565–584.
[24] O. Lopez-Pamies, A new $I_1$-based hyperelastic model for rubber elastic materials, C. R. Mec. 338 (2010) 3–11.
[25] A. Mielke, Necessary and sufficient conditions for polyconvexity of isotropic functions, J. Convex Anal. 12 (2005) 291–314.
[26] J.M. Ball, Convexity conditions and existence theorems in nonlinear elasticity, Arch. Ration. Mech. Anal. 63 (1977) 337–403.
[27] S. Müller, S.J. Spector, An existence theory for nonlinear elasticity that allows for cavitation, Arch. Ration. Mech. Anal. 131 (1995) 1–66.
[28] J. Sivaloganathan, S.J. Spector, On the symmetry of energy minimizing deformations in nonlinear elasticity I: incompressible materials, Arch. Ration. Mech. Anal. 196 (2010) 363–394.
[29] L. Zee, E. Sternberg, Ordinary and strong ellipticity in the equilibrium theory of incompressible hyperelastic solids, Arch. Ration. Mech. Anal. 83 (1983) 53–90.
[30] A.N. Gent, B. Park, Failure processes in elastomers at or near a rigid inclusion, J. Mater. Sci. 19 (1984) 1947–1956.
[31] K. Cho, A.N. Gent, P.S. Lam, Internal fracture in an elastomer containing a rigid inclusion, J. Mater. Sci. 22 (1987) 2899–2905.
[32] J. Moraleda, J. Segurado, J. Llorca, Effect of interface fracture on the tensile deformation of fiber-reinforced elastomers, Int. J. Solids Struct. 46 (2009) 4287–4297.
[33] J.C. Michel, O. Lopez-Pamies, P. Ponte Castañeda, Triantafyllidis, Microscopic and macroscopic instabilities in finitely strained fiber-reinforced elastomers, J. Mech. Phys. Solids 58 (2010) 1776–1803.
[34] C. Cheng, A. Hiltner, E. Baer, Cooperative cavitation in rubber-toughened polycarbonate, J. Mater. Sci. 30 (1995) 587–595.
[35] A.C. Steenbrink, E. Van der Giessen, On cavitation, post-cavitation and yield in amorphous polymer-rubber blends, J. Mech. Phys. Solids. 36 (1999) 732–765.
[36] M.L. Williams, R.A. Schapery, Spherical flaw instability in hydrostatic tension, Int. J. Fract. Mech. 1 (1965) 64–72.